Review of the influence of noise in X-ray computed tomography measurement uncertainty

Ángela Rodríguez Sánchez[1], Adam Thompson[1], Lars Körner[1], Nick Brierley[2] and Richard Leach[1]
[1]Manufacturing Metrology Team, Faculty of Engineering, University of Nottingham, UK
[2]The Manufacturing Technology Centre, Antsy Park, Coventry CV7 9JU, UK

Abstract. Different aspects of noise in X-ray computed tomography (XCT) for industrial purposes are examined. An overview of the most common noise metrics is given, together with a description of XCT noise influence quantities. We address the current state of the art in understanding the contribution of noise to XCT measurement uncertainty, giving a chronological view of the different attempts that have been made to account for the contribution from noise to XCT measurement uncertainty. We conclude that approaches to estimating the contribution of noise to XCT measurement uncertainty that account for not only noise, but also other factors that affect image quality (e.g., scattering, beam hardening and blurring) are preferable to approaches that only account for noise.

1. Introduction

X-ray computed tomography (XCT) is an image acquisition technique based on the interaction of radiation and matter [1]. XCT uses the information provided by the attenuation of X-rays through an object to reconstruct a two- or three-dimensional (2D or 3D, depending on the specific XCT system) representation of the object being measured [2–4]. XCT was introduced for medical imaging purposes in the early 1970s [5] and, although some attempts to apply this technology for non-destructive-testing [6] and dimensional measurements [7,8] were performed at the end of the last century, XCT has only been considered a viable tool for these purposes in the last ten years [2,9]. The introduction of XCT into the field of metrology is justified by the advantages it brings compared to other types of coordinate measuring systems (CMSs), such as tactile or optical CMSs. XCT offers a high measurement point density and is the only CMS capable of non-destructively determining the external and internal geometries of an object, as well as distinguishing between different materials. As such, XCT is now considered a multi-purpose non-destructive testing and measurement technique that allows for simultaneous material testing and dimensional quality control.

One of the main issues with using XCT for dimensional measurements in industry and research is the evaluation of measurement uncertainty [2,10–12]. The difficulties of XCT measurement uncertainty evaluation arise from its plethora of error sources, relating not only to the system itself, but to the operator settings, the object, the data processing and the environmental conditions during the scan [13]. To apply XCT in dimensional quality control scenarios [14], with applications in aerospace [15], automotive [16] and medical [17] industries, traceability of measurements to the SI unit of length (i.e. the metre) is required [18]; thus, evaluation of the uncertainty of XCT measurements is required. Although many attempts have been made to find a method to evaluate XCT measurement uncertainty [19–30], a definitive, standardised method, applicable in measurement laboratories and industrial environments, has not yet been established. The closest a document has achieved so far is VDI/VDE 2630-2.1 [25] – while many consider this document to be a standard, the VDI/VDE documents are intended to act as guidelines, as opposed to explicit standards. The uncertainty evaluation methods

used most widely in the literature are the analytical approach stated in the *Guide to the Expression of Uncertainty in Measurement* (GUM) [31],the GUM simulation approach using Monte Carlo methods [32] and the so-called substitution method. The substitution method is used to estimate the bias contribution of XCT (or indeed any CMS) measurement uncertainty using reference objects that are geometrically and materially similar to the object being measured and have previously been calibrated e.g. by a tactile CMS [22]. Calibration uncertainty is evaluated, and then combined with other influence quantities (e.g. repeatability, thermal effects) to provide the measurement uncertainty. Generic details of the substitution method are addressed in ISO 15530-3 [33] and guidance for its implementation to XCT measurements is given in VDI/VDE 2630-2.1 [25]. However, the substitution method is not generalizable to dissimilar workpieces due to the stringent similarity conditions with respect to the calibrated reference.

One of the XCT measurement uncertainty influence quantities is noise [34]. Thus, when following GUM methods, the contribution of noise to measurement uncertainty must be considered, estimated and then combined with the other influence quantities to form an overall evaluation of uncertainty and ultimately achieve traceability. In the early stages of XCT research, noise was defined as "everything that is unwanted in the image" [35]. However, it is now considered that imaging artefacts are everything unwanted in the image, and noise is but one of these imaging artefacts. Other examples of imaging artefacts include ring artefacts, cone-beam artefacts or artefacts produced by beam hardening and scattering [2]. Noise is currently defined in several publications as unwanted variation of intensity across an X-ray projection [34] and arises from the finite number of detected photons, the object characteristics (e.g. attenuation coefficient and penetration lengths) and the instrumentation and measurement setup used (e.g. X-ray settings, averaging and filtering) [36,37].

In this review, the state of the art in understanding the contribution of noise to XCT measurement uncertainty is summarised. Noise metrics used in dimensional XCT are explained (see section 2) as are the influence quantities that contribute to noise (see section 3). In section 4, an overview of research that has studied the noise contribution to XCT measurement uncertainty is presented. A discussion of the contributions of this research is provided in section 5, together with our perspective. In section 6, the conclusions of the review are presented.

In this review, investigations carried out with the aim of calculating the overall XCT measurement uncertainty [19–30] are not covered, with the exception of those that have directly addressed the contribution from noise. Additionally, while the purpose of the majority of publications related to noise in XCT images is to reduce noise so as to achieve better image quality [38–40], examination of this topic is beyond the scope of this review.

2. Noise measurements

Appropriate metrics for measuring noise in XCT acquisitions have been discussed widely since the introduction of XCT in medicine [35,41–44]. Despite the long duration of this discussion, no definitive metric has emerged in either the medical or the industrial XCT communities. However, while no consensus has been formed, many such metrics have been proposed. In this section, we present and compare the most common and promising noise metrics.

It is worth mentioning that noise can be measured at various points during an XCT measurement: in the 2D projections taken by the XCT system, in the 3D reconstructed volume or in a 2D slice of the reconstructed volume (often called XCT image). In the first case, the projections are comprised of 2D

pixels, and in the other two cases, the reconstructed volumes and the images are comprised of 3D voxels.

2.1 Signal-to-noise and contrast-to-noise ratios

Signal-to-noise ratio (SNR) and contrast-to-noise ratio (CNR) are the most frequent image quality indicators used in signal processing. Definitions for each are provided in numerous books and specification standards [1,45–47] and, although they have multiple definitions, the most common are presented below.

The SNR is defined as the ratio between image signal and image noise [45,47], and is given by

$$SNR = \frac{\bar{g}_{object}}{\sigma_{object}} \qquad (1)$$

while the separation of the object from the background is assessed using the CNR [45], given by

$$CNR = \frac{\bar{g}_{object} - \bar{g}_{background}}{\sigma_{background}} \qquad (2)$$

In both equations, $\bar{g}_{object}$ and $\bar{g}_{background}$ represent the mean grey level of two regions of interest (ROIs) chosen inside and outside the object respectively, and σ_{object} and $\sigma_{background}$ are the standard deviations over the same ROIs.

Both SNR and CNR have been widely used to quantify, optimise and simulate noise in industrial XCT measurements [47–55]. CNR is suggested as a method of quantifying optimal scan settings in ISO 15708-2 [45]. In this standard, selection of scan parameters according to a minimal X-ray transmission of 14% during the scan is suggested. Transmission is defined as the ratio between the radiation intensity before an attenuation and the intensity after that absorption [45].

In practice, the use of user-defined ROIs often requires expert knowledge to avoid misleading results due to imaging artefacts [56], and assumes that the signal is constant in the chosen ROI. Additionally, SNR and CNR do not completely characterise noise, as neither metric is able to account for the spatial frequency distribution of the noise [57]. Figure 1 shows two images with the same SNR, but which have different spatial frequency distributions [58], and thus, appear completely different to the observer. As such, other metrics have been developed for the purposes of eliminating the two main drawbacks of SNR and CNR: ROI dependence and noise spatial frequency distribution independence.

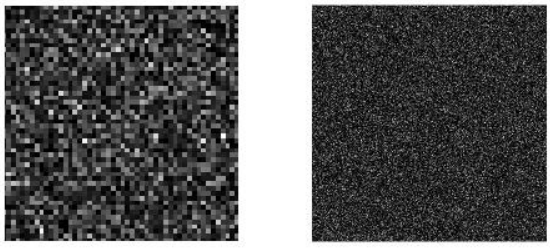

Figure 1: XCT images with same SNR but different noise spatial frequency distribution.

2.2 Noise power spectrum

The noise power spectrum (NPS) describes the noise response of a system as a function of its spatial frequency [42]. The NPS is evaluated over *N* ROIs and is given by

$$\mathrm{NPS} = \frac{1}{N}\sum_{i=1}^{N} |F[I_i(x,y,z) - \overline{I_i}]|^2 \frac{\Delta_x \Delta_y \Delta_z}{N_x N_y N_z} \qquad (3)$$

where I_i is the grey value of each voxel in the ROI i, $\overline{I_i}$ is the mean signal in that ROI, F is the Fourier transform operator, $\Delta_{x,y,z}$ are the voxel dimensions in directions x, y and z, and $N_{x,y,z}$ are the dimensions of each ROI in voxels [57]. Equation (3) can be normalised to obtain the normalised NPS, which has units of metres squared.

In the medical literature, the NPS is evaluated by scanning a homogeneous part, which is typically a water or polymer 'phantom' (a specially designed object that is scanned to evaluate and analyse the performance of imaging systems) [59,60]. NPS has been used to characterise the noise behaviour of XCT systems for different dosimetric quantities (a measure of the ionising radiation absorbed by a body), reconstruction kernels (a process applied to modify the frequency of projection data before image reconstruction [61]) and numbers of projections [57,61]. NPS has also been used to study the dependence of noise on detector characteristics [62] and to compare different XCT systems [63]. However, the NPS, as a Fourier-based method, assumes statistical stationarity. This assumption is violated in real XCT systems, as it is known that noise is not statistically spatially constant across an image (see section 3.1), so some residual systematic errors are to be expected. Some studies have been carried out with the aim of quantifying the non-stationarity of XCT systems and some alternative metrics, such as a spatial approach based on the object transfer matrix and the covariance matrix, have been proposed [64]. However, the use of such metrics is not as common as the use of the NPS.

Due to the non-stationarity of XCT noise, there is an ongoing discussion about the use of local or global NPS to measure image quality (see Hiller et al. [65], who used aluminium cylinders to demonstrate that the NPS and, therefore, the noise level, changes along the rotation axis). This topic will be further discussed in section 3.1

2.3 Full-reference metrics

For some specific studies, where the aim is to compare an XCT image to a reference image of higher quality, techniques known as full-reference metrics have been used [66]. The main parameters used for this purpose are the root-mean-square error (RMSE), the peak SNR (PSNR) and the structural similarity index (SSI). These three metrics were used, e.g., by Villarraga-Gómez to study the effect of the number of projections on XCT image quality [67]; the conclusions of this investigation are discussed in section 3.6.

2.3.1 Root-mean-square error

The RMSE is the square root of the mean of the squared signal intensity difference between each voxel in the test image and its equivalent in the reference image, given by

$$\mathrm{RMSE} = \sqrt{\frac{1}{MN}\sum_{i=1}^{M}\sum_{j=1}^{N}\big(x(i,j) - y(i,j)\big)^2} \qquad (4)$$

where $x(i,j)$ represents the grey level of a specific voxel in the reference image and $y(i,j)$ represents the grey level of the same voxel in the test image. M and N are the total number of voxels in the horizontal and vertical directions respectively. If the RMSE is zero, the test image and the reference image are identical, so a higher value of the RMSE means greater discrepancy.

RMSE has some attractive features: it is simple, it allows for consistent and direct interpretations of similarity and it has a clear physical meaning [68]. Nevertheless, it appears not to behave well when the RMSE is used to predict human perception of image quality. Images with very similar RMSE values can present quite different visual quality, and images that have slight geometrical deviations (e.g. spatial shifts, rotations) have large RMSE values but present acceptable image quality to humans [68,69].

2.3.2 Peak signal-to-noise ratio

The PSNR is used when the images being compared have different dynamic ranges. PSNR is given by

$$\mathrm{PSNR} = 10 \cdot \log_{10}\frac{m}{\mathrm{MSE}} \qquad (5)$$

where m is the maximum value of the signal in the test image and MSE is the mean square error ($\mathrm{MSE} = \mathrm{RMSE}^2$). The higher the PSNR, the greater the similarity between the two images being compared. The ideal case would be represented by a PSNR value of 100 dB, but typically the PSNR lies between 30 dB and 40 dB [66,69–71]. The PSNR metric has the same benefits and limitations as RMSE.

2.3.3 Structural similarity index

Due to the limitations of the RMSE given in section 2.3.1, the SSI was proposed [72] and later formally developed into an alternative metric [69,73]. The SSI represents image quality by combining three factors: luminance distortion, contrast distortion and loss of correlation [73]. Detailing the maths to describe SSI requires extensive discussion and is beyond the scope of this publication, but such a discussion can be found elsewhere [69,73]. The SSI is evaluated using a sliding window that moves voxel by voxel. A metric for the overall image quality is then obtained by calculating the mean of the voxel-by-voxel SSI values (MSSI). If the test image is identical to the reference image, the MSSI is equal to unity.

Studies have shown that the SSI metric is more capable of providing a value which represents the human perception of image quality when compared to MSE and PSNR; while MSE and PSNR can have very similar values for very different visual qualities, SSI shows an agreement between its value and the visual quality of the studied images [68,74]. However, it has also been demonstrated that the SSI is highly sensitive to alignment errors (i.e. relative translation, scaling and rotation) of images [68].

2.4 Other metrics

Other, less commonly used metrics have been proposed to quantify noise in XCT images. Reiter et al. [56] proposed a histogram-based image quality metric *Q* aimed at eliminating the user dependence of other metrics, such as SNR or CNR. *Q* is a measure of the degree of separation of the different material classes in the grey value histogram of the image, and is given by

$$Q = \frac{|\mu_2 - \mu_1|}{\sqrt{\sigma_1^2 + \sigma_2^2}} \qquad (6)$$

where $\mu_{1,2}$ are the mean values of the background and material peaks in the grey value histogram (of a single material scan) and $\sigma_{1,2}$ are their standard deviations.

Further information regarding the calculation of *Q* can be found in [56], where its sensitivity to noise, imaging artefacts, blurring levels and correction techniques is studied.

Schielein et al. [75] performed a quantitative evaluation of the image quality of XCT images using Shannon entropy (SE), defined as

$$H = (-1)\sum_{i}^{N} p_i \log_2 p_i \qquad (7)$$

where p_i are the normalised histogram values of an XCT image with *N* different grey values.

The SE is a measure of information disorder; a lower value indicates a higher image quality, which implies lower noise. Schielein et al. showed that SE is a more reliable indicator of imaging artefacts compared to SNR, since SE shows a clear relationship to the prefiltration and the source current, while SNR does not [71].

Noise metrics are often combined with resolution metrics to create parameters capable of defining image quality. This approach is justified by the fact that it is problematic to compare noise metrics across images with different spatial resolutions. Gang et al. [76] proposed the use of a detectability index, which combines the NPS with the modulation transfer function (MTF). The MTF is a resolution metric that describes how the amplitude of a sinewave is reproduced in an imaging system, with respect to the spatial frequency of the sinewave [77]. For an incoherent imaging system, the MTF is given by the Fourier transform of the point spread function. Gang et al. [73] used the detectability index to study the non-stationary aspects of signal and noise transfer characteristics in XCT images for different reconstruction algorithms [76]. The detectability index was later used by Fischer et al. [78] as a tool to optimise object-specific trajectories.

Other type of image quality metrics are the so-called model observers. Model observers have been used to optimise and assess XCT systems, among other imaging devices [79]. These methods define image quality in terms of how well the information of interest can be extracted from the image according to a specific observer (either a human or a mathematical model) [80]. Among them, it is worth highlighting the ideal observer (IO) model and the pre-whitening (PW) observer model.

In the IO model, the IO is defined as “the observer that utilises all statistical information available regarding the task to maximise task performance as measured by Bayes risk or some other related

measures of performance" [81]. This model uses the likelihood ratio (LR) of the raw data as a decision variable between two hypotheses. The LR is defined as

$$\Lambda(\boldsymbol{g}) = \frac{f(\boldsymbol{g}|H_1)}{f(\boldsymbol{g}|H_0)} \qquad (8)$$

where $\boldsymbol{g}$ is the raw data vector and $f(\boldsymbol{g}|H_i)$ is the probability density function of the image vector under the i^{th} hypothesis [79]. This parameter offers an upper bound against which other observers can be compared. The use of this model implies a high computational burden, which is a significant drawback.

The PW observer conducts the detection by cross-correlation of the image data and a template. The template spatial function allows simultaneous compensation for noise correlations and signal detection [82]. The observer performance is characterised by the detectability index, defined as

$$(d')^2 = \int \frac{S^2(f)}{\mathrm{NPS}^2(f)} f df \qquad (9)$$

where f is the signal, $S(f)$ its amplitude spectrum and $\mathrm{NPS}(f)$ its noise power spectrum [83].

3. Influence quantities

Noise in XCT images is influenced by a large number of quantities relating to the scan settings, the X-ray detector, the object being measured, the reconstruction method and the data processing employed. The main influence quantities are presented in Figure 2 and described in the following sections.

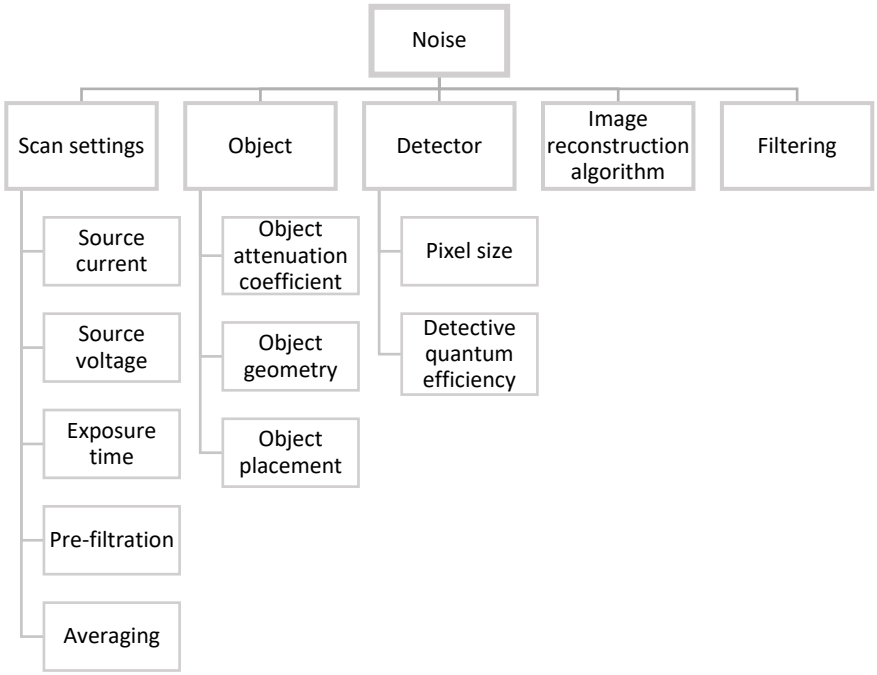

Figure 2 Main influence quantities of XCT image noise.

3.1 Number of detected photons

One of the contributions to the image noise is the shot noise (or quantum noise). The shot noise arises from the quantum nature of the X-ray beam: it consists of individual photons that are spatially distributed according to the Poisson law. This distribution implies fluctuations in the number of photons reaching different regions of the detector, generating a 'graininess' in the image. The quantum noise (σ) is inversely proportional to the square root of the number of photons N[84]:

$$\sigma \propto {}^{1}/_{\sqrt{N}} \qquad (10)$$

Thus, factors that alter the number of detected photons influence the quantum noise by extension. These factors are:

- *Source current:* in the X-ray source of a conventional X-ray tube, a cathode is heated by some electrical current. Due to the thermoelectric effect, electrons exit from the cathode. The number of exiting electrons is proportional to the current: the higher the current, the higher the number of electrons. These electrons are then used to generate X-rays: the higher the number of electrons, the higher the number of photons [1]. Therefore, higher source currents imply a greater number of detected photons. As the number of photons is linearly related to the current, increasing the current reduces image noise by an amount proportional to $1/\sqrt{I}$, where I is the current [85].
- *Source voltage:* the source voltage accelerates electrons exiting from the cathode, increasing their energy. The energy of the electrons that generate photons in the anode is directly related to the peak energy of the generated photons. Photons with higher energy are more likely to penetrate the object [1]. Therefore, higher voltages should increase the number of detected photons. However, the photon generation efficiency in the anode also depends on the voltage, and the detection efficiency decreases with increasing photon energy, giving rise to a complex relationship

between source voltage and noise level. Increasing the voltage reduces image noise by an amount proportional to $\sim V^{1.3}$, where V is the voltage [86].

- *Exposure time:* increasing the exposure time will increase the number of detected photons per pixel. [25] Given the direct equivalence of both current and exposure time with the number of photons, the current-time product is often used as an indicator of image quality [87,88]. As the number of detected photons is linearly related to the exposure time, the exposure time improves image noise by an amount proportional to $1/\sqrt{t}$, where t is the exposure time [85].
- *Pre-filtration:* physical filters are normally used to decrease beam hardening artefacts. Most commonly, pre-filters consist of a few tenths of a millimetre to a few millimetres of copper or aluminium, placed between the X-ray source and the scanned object [34]. This kind of filtration absorbs photons with lower energies to transform the X-ray spectrum. However, as the number of photons is reduced, the noise is increased [13]. The relationship between number of detected photons and noise is given by equation (10), and the number of photons not attenuated by the filter is given by the Beer-Lambert equation

$$N = N_0 e^{-\mu l} \qquad (11)$$

where N_0 is the number of incident photons, μ is the attenuation coefficient of the filter and l is the length travelled through the material (in this case, the filter thickness).

- *Object attenuation coefficient:* the linear attenuation coefficient of any particular material μ is a constant that describes the fraction of attenuated photons in a monoenergetic beam per unit thickness of a specific material [89]. A higher attenuation coefficient implies a higher fraction of attenuated photons and a lower fraction of detected photons, so scans of objects with high μ are noisier than scans of objects with low μ, under the same scan settings. The μ of a specific material decreases with the photon energy, so, as explained above, increasing source voltage will decrease noise level, but at the expense of lowering contrast. The relationship between attenuation coefficient and number of non-attenuated photons is given by equation (11), so decreasing the attenuation coefficient decreases the noise level by an amount proportional to $\sim 1/\sqrt{e^{-\mu l}}$, where l is the object penetration length.
- *Object penetration length:* the attenuation of a photon beam exponentially depends on the length travelled through the attenuating material – see equation (11) [89]. Thus, the longer the distance travelled through the object, the more photons are attenuated, and the greater the resulting noise. Reiter et al. [90] studied both SNR and CNR for the different penetration lengths of an aluminium step cylinder, showing the dependence between travelled length and noise. The dependence between penetration length and noise level implies that, for this reason alone, noise will vary spatially across a volume [91], giving rise to the non-stationarity of noise (see section 2.2). Stationarity is normally used for the temporal domain; however, the term non-stationarity has been widely used in the literature to name the spatial variation of noise across XCT images [90,92–94], and so is used here. The non-stationarity noise characteristics of XCT images have been known since the end of the 20th century [92]. While well studied, non-stationarity is still a major challenge in the assessment of image quality [76]. Local NPS has been used to study noise non-stationarity dependencies [93,94]. Noise varies systematically throughout the axial plane according to changes in the number of detected photons and the finite number of projections. Figure 3 represents the dependence of the axial NPS on the distance from a water cylinder centre. In Figure 3, it is shown that NPS decreases with the radius due to a higher number of detected photons [93]. Other dependencies, such as the tilt angle of the X-rays through the local volume, can be found elsewhere

[94]. To account for these noise variations, the use of local instead of global NPS is suggested [94]. Decreasing penetration length decreases noise level by an amount proportional to $\sim 1/\sqrt{e^{-\mu l}}$.

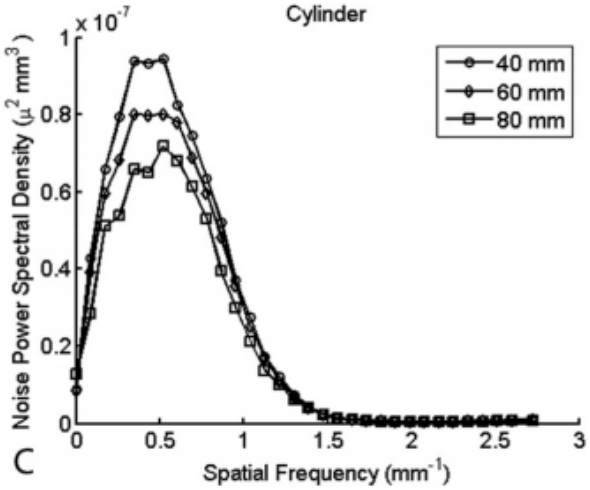

Figure 3 Changes in the axial NPS for different radial distances from the image centre for a water cylinder, showing that the NPS amplitude decreases as a function of radius. Reproduced with permission from [93].

3.2 Detector characteristics

XCT detector characteristics affect both quantum and electronic noise. As quantum noise depends on the number of detected photons per pixel, the larger the pixel, the lower the noise. However, increasing the pixel size compromises other image quality indicators, such as the spatial resolution [86].

The detector itself also adds some noise to the final image, as it does not detect every photon. In XCT, two metrics are used to measure the influence of the detector on the overall noise: noise-equivalent quanta (NEQ) and detective quantum efficiency (DQE). NEQ represents the number of photons at each spatial frequency for which an ideal detector would produce the same NPS, and the DQE describes this value as a fraction of the number of incident photons [95,96]. DQE is also often defined as a measure of the transfer of SNR from the input to the output of the detector [97]62]. There are three main types of detectors: counting-type detectors, scintillation-type (or 'indirect') detectors and ionisation-type detectors. Counting-type detectors provide a response proportional to the number of detected photons and independent to their energy. The output of scintillator-type detectors is proportional to the energy of the detected photons, while ionisation-type detectors measure energy deposition per unit mass [2]. The most widely used XCT detectors are scintillation-type. The scintillators convert the X-ray photons into visible photons, that are detected, in turn, by amorphous silicon photodiode arrays [98]. One of the major factors influencing the DQE is the converter material used (i.e. the component of some type of detectors that convert X-ray photons into visible photons) [65]

The DQE is the most commonly used metric to describe the overall SNR of a detector system. Methods for calculating the DQE of a detector system can be found elsewhere [97,99,100]. DQE is defined as a function of spatial frequency υ as:

$$\mathrm{DQE}(\upsilon) = \frac{\mathrm{MTF}^2 \cdot \phi}{\mathrm{NPS}(\upsilon)} \qquad (12)$$

where ϕ is the X-ray quanta per area in units of photons per metre [65].

It has been demonstrated that the SNR is significantly affected by the energy dependence of the DQE [100,101] and that the DQE of indirect detectors is much less dependent on spatial frequency compared to the other detector types. Unlike counting-type detectors, no uniform dependency of DQE on exposure level has been observed [100]. It has also been shown that the use of detectors with integrated electronics, instead of distributed electronics, substantially reduces the level of electronic noise [102].

3.3 Reconstruction algorithms

The noise in XCT is significantly affected by the chosen reconstruction algorithm [84,86,103]. Some researchers have studied the influence of the use of filtered back projection (FBP) or iterative ordered subsets convex (OSC) maximum-likelihood algorithms on the noise of the reconstructed images. These researchers showed that the OSC method achieves a lower level of noise than the FBP at the same resolution [104,105]. It has also been demonstrated that the reconstruction algorithm affects the non-stationarity of XCT noise (see section 3.1) [34,76]. Noise level is also influenced by some reconstruction algorithm settings, such as the reconstruction kernel or the voxel grid spacing [106,107]. However, these parameters cannot be chosen based only on a desire to decrease noise level, as such choices will likely compromise spatial resolution.

3.4 Filtering

Filtering in XCT is a general term for any kind of operation applied to pixels in the projections or voxels in the reconstructed image (not including pre-filter, as defined in section 3.1) [34]. One of the most common uses of image filtering is noise suppression [108]. The low pass filters are an example of filters used for this purpose. These filters allow passing signals with frequencies lower than a selected value and attenuate signals with higher frequencies [34]. There is a trade-off between high spatial resolution and noise suppression, since filters that only supress very high-frequency signals, will improve spatial resolution, but have a minimal effect on noise, while filters that supress a wider range of frequencies, will decrease noise but deteriorate the spatial resolution [109]. A large number of filters used with the aim of reducing noise can be found in the literature (e.g. Hanning filter [38], median filter with small convolution matrices [110] and neighbourhood sliding filter [111]). The selection of filter type and its parameters has a specific impact on the noise level and its frequency distribution. Studies on how the use of different filters and parameters affects image noise can be found elsewhere [108,112].

3.5 Object placement

Both magnification and workpiece orientation affect image quality and measurement accuracy [2,34]. Theoretically, higher magnifications improve the spatial resolution; however, with increasing magnification the image becomes more blurred. [13]. Object placement also affects penetration length, which is closely related to noise (see section 3.1).

Some studies have focused on determining the optimal object placement, using image quality metrics as indicators [48,113,114]. Amirkhanov et al. [113] developed a method for determining the optimal object orientation in terms of noise. This method is based on the optimisation of penetration lengths and placement stability using a 3D model of the object as an input to estimate imaging artefacts. Grozmani et al. [48] proposed a method for optimising magnification and object orientation for single and multi-material objects. Their algorithm calculates the minimum required photon energy for each orientation by maximising the CNR, to find the placement that minimises the attenuation power of the object.

3.6 Number of projections

It has been demonstrated that noise depends on the number of projections used to reconstruct the XCT image [61,67]. Villarraga-Gómez [67] used full-reference metrics (section 2.3) to study the dependence between image quality and number of projections in simulated and real data. Villarraga-Gómez concluded that, for the workpieces studied, if less than 600 projections are used to reconstruct the image, strong image distortions are to be expected, and that the image quality measures (RMSE, PSNR and MSSI) improve monotonically until 1000 projections is reached [67].

3.7 Averaging

In industrial XCT systems, it is common to have the option to choose the number of images that the XCT scan takes per projection. The number of images taken for a single projection can be averaged and the resultant image is used in the reconstruction process. This technique is based on the fact that shot noise is randomly spatially distributed across the detector pixels, so, by averaging similar images, random fluctuation can be reduced by the square root of the number of images averaged. This technique requires the images being averaged to be acquired under the same conditions (e.g. temperature or X-ray source voltage). Generally, the images being averaged are acquired consecutively. This technique offers better results for well-exposed images, however, for low photon counts, averaging does not offer an advantage, given the output deterioration due to electronic noise.

4. Uncertainty and noise

Although methods to measure and reduce noise in XCT measurements have been investigated, studies into the relationship between noise and measurement uncertainty for typical measurements performed using industrial XCT systems (e.g. lengths, diameters, wall thicknesses, form measurements) are scarce. However, some researchers have proposed different methods to account for the noise contribution in the measurement uncertainty.

Müller et al. [50] studied the influence of image quality (spatial resolution and voxel noise) in XCT measurement uncertainty. They expressed the noise of the voxels of a 2D slice of the reconstructed volume as

$$\sigma_{pn} = \frac{k \cdot \pi}{s \cdot \sqrt{V}} \cdot \frac{1}{\sqrt{I \cdot t \cdot i}} \qquad (13)$$

where k is a constant depending on the back-projection filter type, s is the voxel size of the 2D slice of the reconstructed volume, V represents the number of projections, I is the X-ray source current, t is

the integration time of the detector and i the number of averaged images [115,116]. Müller et al. measure sphere-to-sphere distances on an XCT ball plate and conclude that noise appears not to be significant for the standard deviation of this type of length measurement, while the spatial resolution is the dominant factor. Additionally, they validated the theoretical formulation of voxel noise by analysing the SNR of the images and showed that higher noise values correspond to lower SNR values.

Cuadra et al. [19,117] proposed a method to evaluate XCT measurement uncertainty for a single voxel of a reconstructed image using a measurement model which quantified the dominant error sources at each step of the scan process, particularly: X-ray generation, transmission, detection and acquisition. This type of approach is called a cascaded system. In this work, eight different sources of noise were characterised by their power spectral density functions: emission variation, current, angular variation, pixel solid angle variation, voltage, attenuation term, intrinsic efficiency of the detector and detector counts. Preliminary results of the model [19] were implemented using theoretical noise inputs from reference [118]. In the latter publication, Cuadra et al. proposed a method for measuring acquisition-specific noise parameters [117]. This model requires seven experimental measurements: characterising the X-ray source intensity, dark field counting noise, temperature fluctuation, electrical potential and current fluctuations; scattering measurements, pixel dynamics parameters and mechanical vibration. Currently, only methods for the characterisation of the X-ray source, thermal sensitivity and mechanical vibration have been presented. These authors suggested that, in the future, methods to perform the other experimental measurements and an extension of the uncertainty model from 0D to higher dimensions should be studied.

Lifton et al. [55] showed that, with knowledge of the point spread function and the CNR of an image, it is possible to estimate surface determination uncertainty for 2D images. Although they considered that extending the method to 3D should be straightforward, no further research for this method has been found.

Kiekens [21] studied the measurement uncertainty using XCT systems using two contributions: uncertainty in the voxel size and uncertainty in the number of voxels. Each of these contributions is in turn divided into a series of sub-contributions. In Kiekens' model, the noise is accounted for in the random error sub-contribution for the uncertainty in the number of voxels. The dependence of this parameter on the amount of surrounding material, the use of beam hardening correction filters, the orientation of the studied feature and its location (internal or external) was studied. Kiekens demonstrated that uncertainty due to random errors during calculation is negligible in some cases but can increase to more than 100 μm for some features and scan conditions [21].

4.1 Recent work on uncertainty and noise

In the past year, a number of studies regarding uncertainty and noise for dimensional XCT have been published. The relationship between image quality and form error has been studied by Matern et al. [51], who examined the relationship between probing error, MTF and NPS for simulated and real scans. The image quality measurements were calculated according to ASTM-E1441-11 and ASTM-E1695-95[119,120]. No correlation was found between form error and NPS (neither for simulated nor for real scans), while larger probing errors were found for lower MTF values. As such, the relationship between resolution and probing error can be predicted but establishing a predictable relationship between probing errors and noise is more complex.

Muller et al. [121] developed a method to assess the surface point quality (SPQ) of XCT measurements without requiring a CAD model. The basic principle for this method was previously published elsewhere [122,123]. The method is based on the calculation of different quality parameters for each discrete point of the determined surface. The outcome is an SPQ, which depends on the influence of noise, blurring, artefacts (e.g. beam hardening or cone beam artefacts) and scattering at this specific point. It was shown that the method can be used to detect the SPQ of objects, such as an aluminium hole plate and two touching steel spheres. Additionally, a qualitative correlation between the SPQ and the random measurement error was demonstrated. These authors determined that the main challenges are the abstract nature of the studied quality parameters and the arbitrary scale of the SPQ values, which does not allow for comparability between measurements [121].

Lifton et al. [124] proposed a method to evaluate the standard measurement uncertainty resulting from a specific surface determination method (ISO-50). The ISO-50 surface determination method is the first segmentation algorithm implemented in dimensional XCT and is based on the establishment of the peak voxel grey value of the background and material in the XCT histogram [125]. The ISO-50 threshold is then the half-way mark between these two peaks, i.e. the 50% interval between the background and the material. While often employed in industry, this surface determination algorithm has major drawbacks, such as low accuracy compared to other surface determination methods or the fact that it is highly influenced by imaging artefacts [126], and by the volume of background in the analysed volume. The presence of noise, beam hardening, scattering and imaging artefacts implies that neither background nor object have a constant grey value, but a range of grey values (see Figure 4). Lifton et al. [124] used the standard deviation of both material and background grey levels to evaluate the standard uncertainty due to the surface determination using the ISO-50 algorithm for both Gaussian and non-Gaussian peak fits. This technique is an alternative method for assessing the contribution from noise (as well as other imaging artefacts) to XCT measurement uncertainty without calculating noise specifically. The method was verified numerically and demonstrated using real scans of three workpieces. Additionally, Lifton et al. showed that the measurement uncertainty due to surface determination is negligible for unidirectional measurements (e.g. sphere centre-to-centre) and an important contribution for the often-called bidirectional measurements (e.g. wall thicknesses or radius) [34].

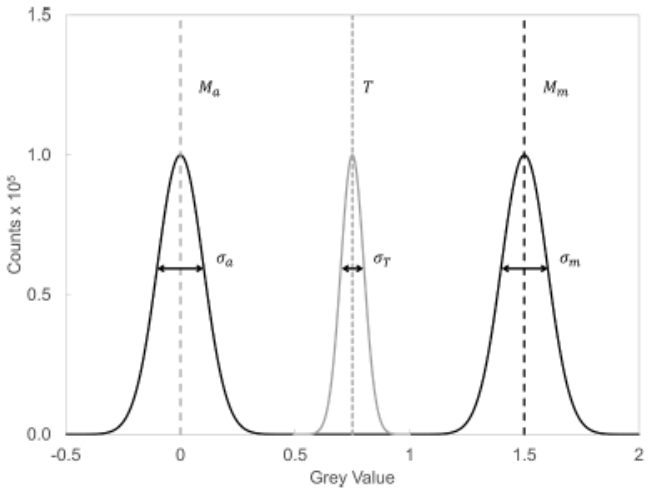

Figure 4 Grey value histogram for a mono-material object. M_a and M_m are the background and material modal grey value, respectively; T, the ISO-50 threshold and σ_x, the standard deviation for the three distributions. Reproduced with permission from [124].

5. Discussion

Noise is one of the most investigated topics in industrial XCT research. However, the majority of research has focused on methods for measuring and decreasing noise, and there has been little research regarding the contribution of noise to measurement uncertainty. Although the volume of research is small, some researchers have studied how noise affects uncertainty of different type of measurements and proposed different ways to estimate its contribution [21,50,51,55,117,121,124].

On the topic of the influence of noise in different types of measurements, it is well known that unidirectional measurements are minimally affected by noise [127,128]. This minimal effect is due to the fact that a large number of points are used to calculate such measures, and that sphere centre-to-centre distance measurements are largely independent of the surface determination method used, although they can be affected by non-stationarity. Conversely, there has been a long-standing assumption that probing errors were more influenced by noise [127], but the authors of a recent publication [51] showed that there is no predictable relationship between probing error and NPS, while a clear relationship can be found between probing error and MTF.

Hence, it is difficult to establish a direct relationship between noise and its corresponding influence on measurement uncertainty for the most common types of measurements carried out in dimensional XCT.

Initial attempts to account for the contribution of noise to XCT measurement uncertainty used analytical expressions or cascaded systems [50,117], but a complete method to evaluate XCT measurement uncertainty due to noise has not yet been developed. Conversely, the latest developments in XCT noise research have been focused on the study of metrics that account not only for noise but also other factors that influence the image quality (e.g. beam hardening, scattering and blurring). The surface point quality metric developed by Muller et al. [121] or the method to evaluate measurement uncertainty due to the ISO-50 surface determination algorithm proposed by Lifton et al. [124] are examples of this trend. Due to the complexity of the relationship between noise and uncertainty of XCT measurements, we consider that such approaches are more suitable for addressing the assessment of noise contribution to XCT uncertainty than methods that attempt to estimate noise contribution alone. However, these approaches have a variety of limitations, mainly due to the fact that they are relatively new, so more research is required to establish a widely-agreed method of calculating XCT measurement uncertainty, which includes its noise contribution.

6. Conclusions

In this paper, we have reviewed the state of the art in noise in dimensional XCT measurements and its contribution to the measurement uncertainty. The main conclusions of this review are:

- A standard metric to measure and study noise in XCT images has not yet been agreed. Classical metrics (e.g. SNR and CNR) have been widely used but found insufficient. Other metrics (e.g. NPS) have been used and shown to be useful in a high number of studies. New metrics that do not have some of the SNR/CNR limitations have been proposed, such as the histogram-based image quality measure (Q).

- Noise in XCT measurements is influenced by many factors relating to scan settings, scanned object, X-ray detector, image reconstruction algorithm and data post-processing. Each influence factor has been discussed and the importance of the non-stationary noise characteristic has been highlighted.
- A limited number of studies into the contribution of noise to XCT measurement uncertainty have been published, though there are a small number of relevant publications. The first studies attempted to model noise using analytical expressions or cascaded systems, but as far as we are aware, no authors have yet proposed a complete method to estimate XCT measurement uncertainty due to noise. Recently, a shift in the way noise contribution is addressed has been found: with the knowledge that noise does not significantly affect unidirectional measurements (e.g. sphere centre-to-centre) and that there is not a predictable trend between noise level and probing errors, methods that study noise contribution together with other image quality parameters (e.g. blurring and imaging artefacts) are considered to be more promising than methods that attempt to estimate the noise contribution to XCT measurement uncertainty alone.

This review justifies the necessity for further research into the noise contribution to XCT measurement uncertainty, as an essential step to achieve traceability of XCT measurements.

Acknowledgements

ARS would like to thank the Engineering and Physical Science Research Council (EPSRC, grant number EP/M008983/1) and the Manufacturing Technology Centre for funding this research. AT would like to thank EURAMET AdvanCT project (project number 17IND08) for funding this work.

References

[1] Kalender W A 2005 *Computed Tomography: Fundamentals, System Technology, Image Quality, Applications* (Publicis Corporate Publishing: Erlangen, Germany)
[2] Kruth J P, Bartscher M, Carmignato S, Schmitt R, De Chiffre L and Weckenmann A 2011 Computed tomography for dimensional metrology *Ann. CIRP* **60** 821–42
[3] De Chiffre L, Carmignato S, Kruth J P, Schmitt R and Weckenmann A 2014 Industrial applications of computed tomography *Ann*. *CIRP* **63** 655–77
[4] Thompson A, Maskery I and Leach R K 2017 X-ray computed tomography for additive manufacturing: a review *Meas. Sci. Technol.* **27** 072001
[5] Hounsfield G 1973 Computerized transverse axial scanning (tomography): Part I. Description of system *Brit. J. Radiol.* **46** 1016–22
[6] Ellingson W A and Vannier M 1988 X-ray computed tomography for nondestructive evaluation of advanced structural ceramics (Materials and Components Technology Division, Aragone National Laboratory (Argonne, USA)
[7] Mitchell K W 1989 A generalized approach to wall thickness measurements in CT images *Topical Proc. Industrial Computerized Tomography* (July, Seattle, USA) 120-4.
[8] Yamazaki K 1992 Three-dimensional cognitive system for quick perception and inspection of mechanical part using computer tomography *Ann. CIRP* **41** 593–6
[9] Carmignato S, Savio E and De Chiffre L 2004 CT techniques for reconstructing 3D geometrical models of complex parts: an approach for traceability establishment and uncertainty evaluation *IMEKO Int. Symp. and Mediterranean Conference on Measurement* (June, Genova, Italy) 387–90
[10] Bartscher M, Sato O, Härtig F and Neuschaefer-Rube U 2014 Current state of standardization in the field of dimensional computed tomography *Meas. Sci. Technol.* **25** 064013

[11] Carmignato S 2012 Accuracy of industrial computed tomography measurements: Experimental results from an international comparison *Ann. CIRP* **61** 491–4
[12] Dewulf W, Kiekens K, Tan Y, Welkenhuyzen F and Kruth J P 2013 Uncertainty determination and quantification for dimensional measurements with industrial computed tomography *Ann. CIRP* **62** 535–8
[13] Welkenhuyzen F, Kiekens K, Pierlet M, Dewulf W, Bleys P and Voet A 2009 Industrial computed tomography for dimensional metrology: Overview of influence factors and improvement strategies *International Conf. on Optical Measurement Techniques for Structures and Systems* (September, Antwerpen, Belgium) 1–9
[14] ISO 9001:2015 *Quality management systems – Requirements* (ISO: Geneva, Switzerland)
[15] AS9100D:2016 *Quality management systems – Requirements for aviation, space and defense organizations* (SAE International)
[16] IATF 16949:2016 *Automotive quality management system* (IATF)
[17] ISO 13485:2016 *Medical devices – Quality management systems – Requirements for regulatory purposes* (ISO_ Geneva, Switzerland)
[18] Larrabee R D and Postek M T 1993 Precision, accuracy, uncertainty and traceability and their application to submicrometer dimensional metrology *Solid State Electron.* **36** 673–84
[19] Cuadra A J and Panas R M 2016 A systems approach to quantifying uncertainty in X-ray systems for metrology *ASPE Summer Topical Meeting* (June, Raleigh, United States) 185–9
[20] Nardelli V C, Donatelli G D, Arenhart F A and Porath M C 2011 Uncertainty evaluation of computed tomography measurements using multiple calibrated Workpieces *II International Congress on Mechanical Metrology (CIMMEC)* (September, Natal, Brazil) 1-4
[21] Kiekens K 2017 *Contributions to Performance Verification and Uncertainty Determination of Industrial Computed Tomography for Dimensional Metrology* (PhD thesis, KU Leuven: Leuven, Belgium)
[22] Müller P, Hiller J, Dai Y, Andreasen J L, Hansen H N and De Chiffre L 2014 Estimation of measurement uncertainties in X-ray computed tomography metrology using the substitution method *CIRP J. Manuf. Sci. Tec.* **7** 222–32
[23] Hiller J, Genta G, Barbato G, De Chiffre L and Levi R 2014 Measurement uncertainty evaluation in dimensional X-ray computed tomography using the bootstrap method *Int. J. Pr. Eng Man.* **15** 617–22
[24] Zanini F, Sorgato M, Savio E and Carmignato S 2020 Uncertainty of CT dimensional measurements performed on metal additively manufactured lattice structures *10th Conf. on Industrial Computed Tomography* (February, Wels, Austria)
[25] VDI-VDE 2630-2.1:2015 Computed tomography in dimensional measurement - Determination of the uncertainty of measurement and the test process suitability of coordinate measurement systems with CT sensors. VDI/VDE Society for Metrology and Automation Engineering (GMA), (Dusseldorf, Germany)
[26] Hiller J and Reindl L M 2012 A computer simulation platform for the estimation of measurement uncertainties in dimensional X-ray computed tomography *Measurement* **45** 2166–82
[27] Schmitt R and Niggemann C 2010 Uncertainty in measurement for X-ray computed tomography using calibrated work pieces *Meas. Sci. Technol.* **21** 054008
[28] Müller A M and Hausotte T 2019 Comparison of different measures for the single point uncertainty in industrial X-ray computed tomography *9th Conf. on Industrial Computed Tomography* (February, Padova, Italy)
[29] Wenig P and Kasperl S 2006 Examination of the measurement uncertainty on dimensional measurements by X-ray computed tomography *European Conf. on Non-Destructive Testing* (June, Moscow, Russia) 1–10

[30] Flessner M, Blauhöfer M, Helmecke E, Staude A and Hausotte T 2015 CT measurements of microparts: numerical uncertainty determination and structural resolution *Proc. SENSOR* (May, Nuremberg, Germany) 483–8
[31] GUM 2008 *Evaluation of measurement data — Guide to the expression of uncertainty in measurement* (BIPM: Saint-Cloud, France)
[32] GUM, Suppl. 1 2008 *Evaluation of measurement data – Guide to the expression of uncertainty in measurement – Propagation of distributions using a Mote Carlo Method* (BIPM: Saint-Cloud, France)
[33] ISO 15530-3:2011 *Geometrical product specifications (GPS) — Coordinate measuring machines (CMM): Technique for determining the uncertainty of measurement — Part 3: Use of calibrated workpieces or measurement standards* (ISO: Geneva, Switzerland)
[34] Carmignato S, Dewulf W, Leach R K 2018 *Industrial X-Ray Computed Tomography* (Springer International Publishing: Berlin)
[35] Herman G T 1980 On the noise in images produced by computed tomography *Comput. Gr.* **12** 271–85
[36] Sun W, Brown S and Leach R 2012 *NPL REPORT ENG 32 An overview of industrial X-ray computed tomography* (National Physical Laboratory: London)
[37] Wang J, Lu H, Liang Z, Eremina D, Zhang G, Wang S, Chen J and Manzione J 2008 An experimental study on the noise properties of x-ray CT sinogram data in Radon space *Phys. Med. Biol.* **53** 3327–41
[38] Demirkaya O 2001 Reduction of noise and image artifacts in computed tomography by nonlinear filtration of the projection images *Medical Img: Img Procs.* **4322** 917–23
[39] Yan H and Mou X 2010 Projection correlation based noise reduction in volume CT *IEEE Nuclear Science Symposium & Medical Imaging Conf.* (November, Tennessee, USA) 2948–53
[40] Jiang H, Chen W R and Liu H 2002 Techniques to Improve the Accuracy and to Reduce the Variance in Noise Power Spectrum Measurement *IEEE Trans. Biomed.* **49** 1270–8
[41] Hanson K M 1981 Noise and contrast discrimination in computed tomography *Radiol. Skull Brain* **5** 3941-55
[42] Riederer S J, Pelc N J and Chesler D A 1978 The noise power spectrum in computed X-ray tomography *Phys. Med. Biol.* **23** 446–54
[43] Duerinckx A J and Macovski A 1979 Nonlinear polychromatic and noise artifacts in X-ray computed tomography images *J. Comput. Assist. Tomogr.* **3** 519–26
[44] Faulkner K and Moores B M 1984 Noise and contrast detection in computed tomography images *Phys. Med. Biol.* **29** 329-39
[45] ISO 15708-2:2002 *Non-destructive testing - Radiation methods - Computed tomography – Part 2: Examination practices* (ISO: Geneva, Switzerland)
[46] EN 16016-2:2010 *Non-destructive testing - Radiation methods - Computed tomography* (ISO: Brussels, Belgium)
[47] Buratti A, Grozmani N, Voigtmann C, Sartori L v. and Schmitt R H 2018 Determination of the optimal imaging parameters in industrial computed tomography for dimensional measurements on monomaterial workpieces *Meas. Sci. Technol.* **29** 115009
[48] Grozmani N, Buratti A and Schmitt R H 2019 Investigating the influence of workpiece placement on the uncertainty of measurements in industrial computed tomography *9th Conf. Industrial Computed Tomography* (February, Padova, Italy)
[49] Christoph R, Leinweber C, Fischer A, Weise H, Kachelrieß M, Leinweber C and Kachelrieß M 2019 Validation of a Method for the Optimization of scan parameters for measuring with computed tomography *9th Conf. Industrial Computed Tomography* (February, Padova, Italy)

[50] Müller P, Hiller J, Cantatore A, Bartscher M and Chiffre L de 2012 Investigation on the influence of image quality in X-ray CT metrology 4*th Conf. Industrial Computed Tomography* (September, Wels, Austria)
[51] Matern D and Töpperwien M 2020 How much does image quality influence the form error in industrial X-Ray CT? *10th Conf. Industrial Computed Tomography* (February, Wels, Austria)
[52] Franco L, Yagüe-fabra J A, Jiménez R, Maestro M and Ontiveros S 2014 Error sources analysis of computed tomography for dimensional metrology: an experimental approach *European Conf. Non-Destructive Testing* (October, Prague, Czech Republic)
[53] Arenhart F A, Nardelli V C and Donatelli G D 2016 Comparison of Surface-based and Image-based Quality Metrics for the Analysis of dimensional computed tomography data *Case Stud. Nondest. Test. Evaluation* **6** 111-21
[54] Nardelli V C, Arenhart F A and Donatelli G D 2012 Feature-based analysis for quality assessment of x-ray computed tomography measurements *Meas. Sci. Technol.* **23** 105006
[55] Lifton J J, Malcolm A A and McBride J W 2015 On the uncertainty of surface determination in X-ray computed tomography for dimensional metrology *Meas. Sci. Technol.* **26** 053003
[56] Reiter M, Weiß D, Gusenbauer C, Erler M, Kuhn C and Kastner J 2014 Evaluation of a histogram-based image quality measure for X-ray computed tomography 6*th Conf. Industrial Computed Tomography* (February, Wels, Austria)
[57] The International Commission on Radiation units and Measurements 2012 ICRU Report 87. Noise assessment in CT *Journal of the ICRU* **12** 121–34
[58] MathWorks 2020 MATLAB 2020a (Available at https://uk.mathworks.com/products/matlab.html) Accessed: 12th June 2020
[59] Iturralde M P 1982 *CRC Dictionary and Handbook of Nuclear Medicine and Clinical Imaging* (CRC Press: Florida, USA)
[60] Friedman S N, Fung G S K, Siewerdsen J H and Tsui B M W 2013 A simple approach to measure computed tomography (CT) modulation transfer function (MTF) and noise-power spectrum (NPS) using the American College of Radiology (ACR) accreditation phantom *Med. Phys.* **40** 1–9
[61] Zhao Z, Gang G J and Siewerdsen J H 2014 Noise, sampling, and the number of projections in cone-beam CT with a flat-panel detector *Med. Phys.* **41** 061909
[62] Baek J and Pelc N J 2011 Effect of detector lag on CT noise power spectra *Med. Phys.* **38** 2995–3005
[63] Pahn G, Skornitzke S, Schlemmer H P, Kauczor H U and Stiller W 2016 Toward standardized quantitative image quality (IQ) assessment in computed tomography (CT): A comprehensive framework for automated and comparative IQ analysis based on ICRU Report 87 *Phys. Medica* **32** 104–15
[64] Brunner C C, Abboud S F, Hoeschen C and Kyprianou I S 2012 Signal detection and location-dependent noise in cone-beam computed tomography using the spatial definition of the Hotelling SNR *Med. Phys.* **39** 3214–28
[65] Hiller J, Maisl M and Reindl L M 2012 Physical characterization and performance evaluation of an X-ray micro-computed tomography system for dimensional metrology applications *Meas. Sci. Technol.* **23** 085404
[66] Bovik A 2001 *Handbook of Image and Video Processing* Academic Press Series in Communications, Networking, and Multimedia (San Diego, USA)
[67] Villarraga-Gómez H 2018 *Studies of Dimensional Metrology with X-ray CAT Scan* (PhD thesis, University of North Carolina at Charlotte: Charlotte, USA)
[68] Wang Z and Bovik A C 2009 Mean squared error: Love it or leave it? A new look at signal fidelity measures *IEEE Signal Process. Mag.* **26** 98–117

[69] Zhou W and Bovik A 2006 Modern image quality assessment *Synthesis Lectures on Image, Video, and Multimedia Processing* **2** 1-156
[70] Kotevski Z and Mitrevski P 2010 Experimental comparison of PSNR and SSIM metrics for video quality estimation *International Conf. on Industrial Computed Tomography Innovations* (September, Ohrid, Macedonia) 357–66
[71] Ndajah P, Kikuchi H, Watanabe H and Muramatsu S 2011 An Investigation on The Quality of Denoised Images *Int. J. Circuits, Syst. Signal Process.* **5** 423-34
[72] Wang Z and Bovik A C 2002 A universal image quality index *IEEE Signal Process. Lett.* **9** 81–4
[73] Wang Z, Bovik A C, Sheikh H R and Simoncelli E P 2004 Image quality assessment: From error visibility to structural similarity *IEEE T. Image Process.* **13** 600–12
[74] Sheikh H R, Sabir M F and Bovik A C 2006 A statistical evaluation of recent full reference image quality assessment algorithms image processing *IEEE T. Image Process.* **15** 3441–52
[75] Schielein R, Schröpfer S, Kiunke M, Zabler S and Kasperl S 2014 Quantitative evaluation of CT Images by means of Shannon Entropy *European Conf. on Non-Destructive Testing* (October, Prague, Czech Republic)
[76] Gang G J, Stayman J W, Zbijewski W and Siewerdsen J H 2013 Modeling and control of nonstationary noise characteristics in filtered-backprojection and penalized likelihood image reconstruction *The international Society for optics and photonics (SPIE) Medical Imaging Conf.* (February, Florida, USA)
[77] Flay N and Leach R K 2012 *NPL REPORT ENG 41 Application of the optical transfer function in X-ray computed tomography – a review* (National Physical Laboratory: London)
[78] Fischer A, Lasser T, Schrapp M, Stephan J and Noël P B 2016 Object Specific trajectory optimization for industrial X-ray computed tomography *Sci. Rep.* **6** 1–9
[79] He X and Park S 2013 Model observers in medical imaging research *Theranostics* **3** 774-86
[80] Barrett HH, Yao J, Rolland JP and Myers KJ 1993 Model observers for assessment of image quality *Proc. Natl. Acad. Sci. USA* **90** 9758-65
[81] Barrett HH and Myers KJ 2004 *Foundations of Image Science* (Wiley & Sons: New York, USA)
[82] Harris J 1964 Resolving power and decision theory *J. Opt. Soc. Am.* **5** 606-22
[83] Burgess A 1998 Prewhitening revisited Proc. SPIE 3340, Medical Imaging: Image perception 55-63
[84] Verdun F R, Racine D, Ott J G, Tapiovaara M J, Toroi P, Bochud F O, Veldkamp W J H, Schegerer A, Bouwman R W, Hernandez-Giron I, Marshall N W and Edyvean S 2015 Image quality in CT: From physical measurements to model observers *Phys. Medica* **31** 823–43
[85] Brooks R A and Chiro G 1976 Statistical limitations in X-ray reconstructive tomography *Med. Phys*. **3** 237–40
[86] Hilts M and Duzenli C 2004 Image noise in X-ray CT polymer gel dosimetry *J. Phys. Conf. Ser.* **3** 252–6
[87] Raman S, Mahesh MS, Blasko RV Fishman EK 2013 CT scan parameters and radiation dose: practical advice for radiologists *J. Am. Coll. Radiol.* **10** 840-46
[88] Kalra MK, Maher MM, Toth TL, Schmidt B, Westerman BL, Morgan HT, Saini S 2004 Techniques and applications of automatic tube current modulation for CT *Radiology* **233** 649-57
[89] Huda W and Slone R M 2003 *Review of Radiologic Physics* Lippincott Williams & Wilkins (Philadelphia, USA)
[90] Reiter M, Krumm M, Kasperl S, Kuhn C, Erler M, Weiß D, Heinzl C, Gusenbauer C and Kastner J 2012 Evaluation of transmission based image quality optimisation for X-ray computed tomography 4*th Conf. on Industrial Computed Tomography* (September, Wels, Australia)
[91] Brierley N, Nye B, McGuiness J 2019 Mapping the spatial performance variability of an X-ray computed tomography inspection *Nondestruct. Test. Evaluation Int.* **107** 102127

[92] Hsieh J 1997 Nonstationary noise characteristics of the helical scan and its impact on image quality and artifacts *Med. Phys*. **24** 1375–84
[93] Pineda A R, Tward D J, Gonzalez A and Siewerdsen J H 2012 Beyond noise power in 3D computed tomography: The local NPS and off-diagonal elements of the Fourier domain covariance matrix *Med. Phys.* **39** 3240–52
[94] Baek J and Pelc N J 2011 Local and global 3D noise power spectrum in cone-beam CT system with FDK reconstruction *Med. Phys.* **38** 2122–31
[95] Tward D J and Siewerdsen J H 2008 Cascaded systems analysis of the 3D noise transfer characteristics of flat-panel cone-beam CT *Med. Phys.* **35** 5510–29
[96] Siewerdsen J H, Antonuk L E, Yorkston J, Huang W, Boudry J M, Cunningham I A, Siewerdsen J H, Antonuk L E, Yorkston J, Huang W, Boudry J M and Cunningham I A 1997 Empirical and theoretical investigation of the noise performance of indirect detection, active matrix flat-panel imagers (AMFPIs) for diagnostic radiology *Med. Phys.* **24** 71-89
[97] Granfors P R 2003 DQE Methodology — Step by Step *American Association of Physicist in Medicine (AAPM) 45th Annu. Meeting* (August, San Diego, United States)
[98] Bartscher M, Neuschaefer-Rube U and Wäldele F 2004 Computed tomography - A highly potential tool for industrial quality control and production near measurement *8th Intern. Symp. on Measurement and Quality Control in Production* (November, Erlangen, Germany)
[99] IEC 62220-1-1: 2003 Medical electrical equipment - Characteristics of digital X-ray imaging devices: Part 1. Determination of the detective quantum efficiency - Detectors used in radiographic imaging (IEC: Geneva, Switzerland)
[100] Illers H, Buhr E and Hoeschen C 2005 Measurement of the detective quantum efficiency (DQE) of digital X-ray detectors according to the novel standard IEC 62220-1 *Radiat. Prot. Dosim.* **114** 39–44
[101] Tapiovaara M J and Wagner R F 1986 SNR and DQE analysis of broad spectrum X-ray imaging *Phys. Med. Biol.* **31** 195
[102] Duan X, Wang J, Leng S, Schmidt B, Allmendinger T, Grant K, Flohr T and McCollough C H 2013 Electronic noise in CT detectors: impact on image noise and artifacts *Am. J. Roentgenol*. **201** 626–32
[103] Yang K and Kwan A L C 2008 Noise power properties of a cone-beam CT system for breast cancer detection *Med. Phys.* **35** 5317–27
[104] Ziegler A, Heuscher D, Köhler T, Nielsen T, Proksa R and Utrup S 2004 Systematic investigation of the reconstruction of images from transmission tomography using a Filtered Backprojection and an iterative OSML reconstruction algorithm IEEE *Nuclear Science Symposium Conf. Record* (October, Rome, Italy) 2516–9
[105] Ziegler A, Köhler T and Proksa R 2007 Noise and resolution in images reconstructed with FBP and OSC algorithms for CT *Med. Phys.* **34** 585–98
[106] Shafik-ul-Hassan M, Zhang G G, Hunt D C, Latifi K, Ullah G, Gillies R J, Moros E G 2017 Accounting for reconstruction kernel-induced variability in CT radiomic features using noise power spectra *J. Med. Imaging* **5** 011013
[107] Eldevik K, Norhoy W, Skretting A Relationship between sharpness and noise in CT images reconstructed with different kernels *Radiat. Prot. Dosim.* **139** 430-33
[108] Van Laere K, Koole M, Lemahieu I and Dierckx R 2001 Image filtering in single-photon emission computed tomography: Principles and applications Comput. *Med. Imag. Grap.* **25** 127–33
[109] Lyra M and Ploussi A 2011 Filtering in SPECT image reconstruction *Int. J. Biomed. Imaging* vol. 2011 693795
[110] Stolfi A, Kallasse M-H, Carli L and De Chiffre L 2016 Accuracy enhancement of CT measurements using data filtering *6th Conf. on Industrial Computed Tomography* (February, Wels, Austria)

[111] Zargar S, Phad V, P K and Jon R 2015 Role of filtering techniques in computed tomography (CT) image reconstruction *Int. J. Research Eng. Sci. Technol.* **4** 69–74
[112] Bartscher M, Staude A, Ehrig K and Ramsey A 2012 The influence of data filtering on dimensional measurements with CT *World Conf. of Non Destructive Testing* (April, Durban, South Africa)
[113] Amirkhanov A, Heinzl C, Reiter M and Gröller E 2010 Visual optimality and stability analysis of 3DCT scan positions *IEEE T. Vis. Comput. Gr.* **16** 1477–86
[114] Heinzl C, Kastner J, Amirkhamov A, Gröller E and Gusenbauer C 2012 Optimal specimen placement in cone beam X-ray computed tomography *Nondestruct. Test. Evaluation Int.* **50** 42–9
[115] Hiller J, Fuch T O J and Reindl L M 2011 Influence of the quality of X-ray computed tomography image on coordinate measurements: principles, measurements and simulations *Tech. Mess.* **78** 334–47
[116] ISO 15708-1:2002 Non-destructive testing - Radiation methods - Computed tomography - Part 1: Principles (ISO: Geneva, Switzerland)
[117] Cuadra J, Divin C and Panas R 2017 Uncertainty Quantification of an X-ray Computed Tomography System *European society for Precision Engineering and Nanotechnology (EUSPEN) Special Interest Group Meeting: Additive Manufacturing* (October, Leuven, Belgium)
[118] Panas R M, Cullinan M A and Culpepper M L 2012 Design of piezoresistive-based MEMS sensor systems for precision microsystems *Precis. Eng.* **36** 44–54
[119] ASTM-E1441-11:2011 Standard guide for computed tomography (CT) imaging (ASTM International: West Conshohocken, United States)
[120] ASTM-E1695-95:2013 Standard test method for measurement of computed tomography (CT) system performance (ASTM International: West Conshohocken, United States)
[121] Müller A M, Butzhammer L, Wohlgemuth F and Hausotte T 2020 Automated evaluation of the surface point quality in dimensional X-ray computed tomography *Tech. Mess.* **87** 111–21
[122] Fleßner M, Müller A, Helmecke E and Hausotte T 2015 Automated detection of artefacts for computed tomography in dimensional metrology *Conf. on Digital Industrial Radiology and Computed Tomography* (June, Ghent, Belgium)
[123] Fleßner M, Müller A, Helmecke E and Hausotte T 2014 Evaluating and visualizing the quality of surface points determined from computed tomography volume data *Proc. MacroScale: Recent developments in traceable dimensional measurements* (October, Vienna, Austria)
[124] Lifton J J and Liu T 2020 Evaluation of the standard measurement uncertainty due to the ISO50 surface determination method for dimensional computed tomography *Precis. Eng.* **61** 82–92
[125] Borges de Oliveira F, Stolfi A, Bartscher M, de Chiffre L and Neuschaefer-Rube U 2016 Experimental investigation of surface determination process on multi-material components for dimensional computed tomography *Case Stud. Nondest. Test. Evaluation* **6** 93–103
[126] Tan Y, Kiekens K, Kruth J, Voet A and Dewulf W 2011 Material dependent thresholding for dimensional X-ray computed tomography *International Symposium on Digital Industrial Radiology and Computed Tomography* (June, Berlin, Germany)
[127] Carmignato S and Pierobon A 2011 Preliminary results of the 'CT Audit' project: First international intercomparison of computed tomography systems for dimensional metrology *International Symposium on Digital Industrial Radiology and Computed Tomography* (June, Berlin, Germany)
[128] Carmignato S, Pierobon A, Rampazzo P, Parisatto M and Savio E 2012 CT for industrial metrology – accuracy and structural resolution of CT dimensional measurements 4*th Conf. on Industrial Computed Tomography* (September, Wels, Austria)